

Title	Indoor airborne ultrasonic wireless communication using OFDM methods
Authors	Jiang, Wentao;Wright, William M. D.
Publication date	2017-07-11
Original Citation	Jiang, W. and Wright, W. M. D. (2017) 'Indoor airborne ultrasonic wireless communication using OFDM methods', IEEE Transactions on Ultrasonics, Ferroelectrics and Frequency Control, 64(9), pp. 1345-1353. doi:10.1109/TUFFC.2017.2725583
Type of publication	Article (peer-reviewed)
Link to publisher's version	10.1109/TUFFC.2017.2725583
Rights	© 2017, IEEE. Personal use of this material is permitted. Permission from IEEE must be obtained for all other uses, in any current or future media, including reprinting/republishing this material for advertising or promotional purposes, creating new collective works, for resale or redistribution to servers or lists, or reuse of any copyrighted component of this work in other works.
Download date	2024-04-27 03:27:28
Item downloaded from	https://hdl.handle.net/10468/7266

Indoor Airborne Ultrasonic Wireless Communication Using OFDM Methods

Wentao Jiang, *Student Member, IEEE*, and William M. D. Wright, *Senior Member, IEEE*

Abstract—Concerns still exist over the safety of prolonged exposure to radio frequency (RF) wireless transmissions and there are also potential data security issues due to remote signal interception techniques such as Bluesniping. Airborne ultrasound may be used as an alternative to RF for indoor wireless communication systems for securely transmitting data over short ranges, as signals are difficult to intercept from outside the room. Two types of air-coupled capacitive ultrasonic transducer were used in the implementation of an indoor airborne wireless communication system. One was a commercially available SensComp series 600 ultrasonic transducer with a nominal frequency of 50 kHz, and the other was a prototype transducer with a high- k dielectric layer operating at higher frequencies from 200 kHz to 400 kHz. Binary phase-shift keying (BPSK), quadrature phase-shift keying (QPSK) and quadrature amplitude modulation (QAM) based orthogonal frequency division multiplexing (OFDM) modulation methods were successfully implemented using multiple orthogonal subchannels. The modulated ultrasonic signal packets were synchronised using a wireless link, and a least-squares channel estimation algorithm was used to compensate the phase and amplitude distortion introduced by the air channel. By sending and receiving the ultrasonic signals using the SensComp transducers, the achieved maximum system data rate was up to 180 kb/s using 16-QAM modulation with ultrasonic channels from 55 kHz to 99 kHz, over a line-of-sight transmission distance of 6 m with no detectable errors. The transmission range could be extended to 9 m and 11 m using QPSK and BPSK modulation schemes, respectively. The achieved data rates for the QPSK and BPSK schemes were 90 kb/s and 45 kb/s using the same bandwidth. For the high- k ultrasonic transducers, a maximum data rate up to 800 kb/s with no measurable errors was achieved up to a range of 0.7 m. The attainable transmission ranges were increased to 1.1 m and 1.2 m with data rates of 400 kb/s and 200 kb/s using QPSK and BPSK, respectively.

Keywords— *air-coupled ultrasound; channel estimation; capacitive ultrasonic transducers; orthogonal frequency division multiplexing (OFDM); ultrasonic communication*

I. INTRODUCTION

Radio frequency (RF) based wireless technologies have become prolific in the last few decades. The use of the RF spectrum is strictly regulated to prevent interference between different communication systems [1]. This partly constrains the system flexibility in allocating spectrum resources. In addition, due to the radiative and penetrative nature of RF communications, the signals can be easily intercepted remotely [2], therefore limiting their ability to provide a secure system to ensure confidentiality of information. Furthermore, RF transmissions are inappropriate in some circumstances where communication is required, such as inside intrinsically safe

industrial environments. Long term exposure to RF radiation is also considered as a potential threat to public health as the World Health Organization has classified the emitted RF electromagnetic fields as a possible human carcinogen [3]. Some countries are also restricting the use of RF, for example, in 2015, the Assemblée Nationale in France passed a bill prohibiting the installation of Wi-Fi equipment in areas dedicated to the activities of children under 3 years of age [4].

Unlike RF communications, ultrasonic transmissions use unregulated frequency bands, and can be implemented in relatively simple and low-cost fashion. They may also be a good alternative to RF methods in circumstances where radio emission is prohibited. On the other hand, ultrasonic signals in air are highly localised and do not penetrate easily through solid materials, therefore eliminating unwanted external intervention. The medical experience of therapeutic and diagnostic ultrasound in the last few decades has shown that the use of ultrasound is harmless, as long as the overall acoustic output intensity is limited to safe levels, preventing hazardous bioeffects such as heating and cavitation in tissues [5]. Therefore, the use of ultrasonic technology in wireless communications can be considered as a safe alternative to RF systems for transmitting data more securely.

The use of ultrasonic waves as means of signal transmission in air has been investigated previously by several authors. Ultrasonic data was successfully transmitted and received across a 3-m distance through air at 31 kHz, with a system rate of 75 b/s in [6]. In [7], an indoor data communication system was developed by transmitting 40 kHz frequency-shift keying (FSK) modulated ultrasonic signals. The system achieved a functional range of 10 m with a data rate of 100 b/s. Later work has studied ultrasonic communications over a short distance of 0.5 m using multiple-channel amplitude-shift keying (ASK) and ON-OFF keying (OOK) modulations with a carrier frequency of 250 kHz [8]. In this work, a pair of laboratory-made prototype ultrasonic transducers was used, achieving a system transfer rate of 80 kb/s. In [9], the authors compared the performances of OOK, binary frequency-shift keying (BFSK) and binary phase-shift keying (BPSK) modulation schemes used for transmitting ultrasonic signals across an air gap. The maximum system bit rate used was 83 kb/s at a range up to 1.6 m without decoding errors. Another later study by the same authors has looked at the implementation of quadrature phase-shift keying (QPSK) modulation at a higher bit rate of 200 kb/s over 1.2 m [10]. The previous works indicate that most ultrasonic communication systems have suffered from either limited data rates or short transmission ranges. The aim of this work was to investigate more efficient and reliable airborne wireless ultrasonic communication methods using advanced orthogonal frequency division multiplexing (OFDM)

modulation algorithms, achieving more practical data transfer rates and transmission ranges in an indoor environment. Note that this article is an extension of the previously published International Ultrasonics Symposium paper [11]. In Section II, the implementation of the OFDM system including signal modulation, demodulation, channel estimation and synchronization technique is described. This is followed by the apparatus used and experimental layout of the work in Section III. Section IV and Section V give the experimental results and the conclusions, respectively.

II. SYSTEM DESCRIPTION

A. OFDM modulation and demodulation

OFDM is a special form of multicarrier method that distributes data over a number of equal-bandwidth narrow frequency channels. To maintain the orthogonality among all the subcarrier signals over the symbol duration T_s , the symbol rate $1/T_s$ was chosen to be equal to the separation f_d of the neighbouring subcarriers. The use of orthogonal subcarriers allows subchannel spectra to overlap, thus eliminating unnecessary guard bands and significantly increasing the spectral efficiency. A typical baseband OFDM signal, $s(t)$, can be expressed as the sum of N modulated subcarriers

$$s(t) = \sum_{k=0}^{N-1} s_k e^{j2\pi k f_d t} \Pi(t), \quad (1)$$

$$\Pi(t) = \begin{cases} 1, & 0 < t \leq T_s \\ 0, & \text{otherwise.} \end{cases} \quad (2)$$

Here s_k represents the OFDM symbol. Each transmitted symbol s_k is assigned with one of M possible signal states, and can be denoted as $s_k \in [s^{(1)}, s^{(2)}, \dots, s^{(M)}]$. For example, $M = 4$, if QPSK modulation is applied. $\Pi(t)$ represents a rectangular pulse with a duration of T_s . This rectangular window in the time domain produces a sinc-shape spectrum in the frequency domain which makes the subcarriers heavily overlap each other without any intercarrier interference. Due to the orthogonal nature of each subcarrier signal, the OFDM symbols, s_k , can be detected by

$$s_k = \frac{1}{T_s} \int_0^{T_s} s(t) e^{-j2\pi k f_d t} dt \quad (3)$$

at the receiver if there is no channel distortion introduced.

The block diagram of OFDM modulation and demodulation is illustrated in Fig. 1. In practice, the encoded bits in series are mapped onto a modulation constellation producing complex values that represent the modulated subcarriers in parallel. The modulation and multiplexing can then be achieved digitally using an inverse fast Fourier transform (IFFT) as (1) can be expressed by

$$s\left(\frac{nT_s}{N}\right) = \sum_{k=0}^{N-1} s_k e^{j\frac{2\pi}{N} k f_d n T_s} = \sum_{k=0}^{N-1} s_k e^{j\frac{2\pi}{N} k n}, \quad (4)$$

where T_s/N is the sample interval and $n = 0, \dots, N-1$. The OFDM demodulation is virtually the inverse operation of the

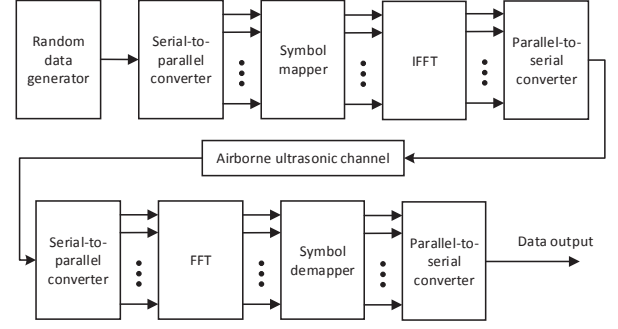


Fig. 1. Block diagram of OFDM modulation and demodulation.

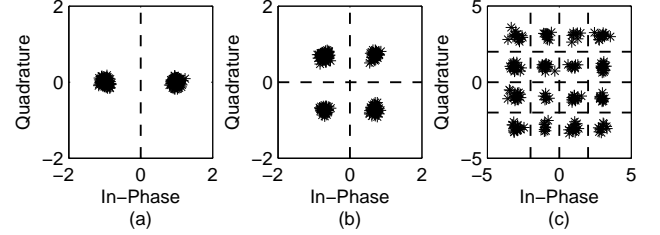


Fig. 2. Simulated OFDM signal constellation diagrams for an SNR of 5 dB. (a) BPSK, (b) QPSK, and (c) 16-QAM. The detection boundaries are indicated by dashed lines.

modulation. The fast Fourier transform (FFT) processing block transforms the OFDM symbols from the time domain to the frequency domain before demapping them to the corresponding constellation patterns.

Fig. 2 show three constellation diagrams of the received OFDM signals using BPSK, QPSK and 16-quadrature amplitude modulation (16-QAM) with a signal-to-noise ratio (SNR) of 5 dB in simulation. As can be seen, after introducing additive white Gaussian noise (AWGN), the demapped OFDM symbols are scattered around their target points, but all the constellation points are grouped and well separated. As long as no demapped symbol across the detection boundaries, all the transmitted bits can be correctly decoded. Note that all three of these modulation techniques were studied in the OFDM communication system in this work.

B. Channel estimation

As OFDM is highly sensitive to frequency and phase noise, pilot symbols are added to the data packet. They are used to estimate the channel transfer function, and the inverse is applied to every subcarrier OFDM signal to compensate for the channel, so that OFDM can simplify the equalization process by turning the frequency-selective channel into a flat channel. During demodulation, the pilot subcarriers that were known by the receiver are used to correct the phase and amplitude of the received OFDM signals.

Assuming that the channel is with AWGN, the continuous-time received signal $r(t)$ in such a system is given by

$$r(t) = s(t) * c(t) + n(t), \quad (5)$$

where $s(t)$ is the transmitted pilot signal, $c(t)$ is the channel impulse response, and $n(t)$ is the noise signal. In matrix form, (5) can be rewritten as

$$\mathbf{r} = \mathbf{S}_p \mathbf{c} + \mathbf{n}, \quad (6)$$

where the received signal vector \mathbf{r} , channel frequency response vector \mathbf{c} and the noise signal vector \mathbf{n} are given as

$$\mathbf{r} = \begin{bmatrix} r_0 \\ \vdots \\ r_{N-1} \end{bmatrix} \quad \mathbf{c} = \begin{bmatrix} c_0 \\ \vdots \\ c_{N-1} \end{bmatrix} \quad \mathbf{n} = \begin{bmatrix} n_0 \\ \vdots \\ n_{N-1} \end{bmatrix}$$

and \mathbf{S}_p which is referred to the pilot matrix is defined as

$$\mathbf{S}_p = \begin{bmatrix} s_0 & 0 & \cdots & 0 \\ 0 & s_1 & \ddots & 0 \\ \vdots & \ddots & \ddots & \vdots \\ 0 & \cdots & 0 & s_{N-1} \end{bmatrix}.$$

Given the vector \mathbf{r} and the matrix \mathbf{S}_p , the pilot-aided channel estimation technique is to find an estimate $\hat{\mathbf{c}}$ of the channel vector \mathbf{c} . This can be achieved by using maximum likelihood (ML) parameter estimation [12] which is based on finding the value of \mathbf{c} that solves

$$\min_{\mathbf{c}} \|\mathbf{r} - \mathbf{S}_p \mathbf{c}\|^2.$$

It is obvious that the ML estimate of \mathbf{c} is equivalent to the least-squares (LS) estimation algorithm in this case, yielding

$$\hat{\mathbf{c}}_{LS} = \mathbf{S}_p^{-1} \mathbf{r}. \quad (7)$$

C. Frame synchronization

Time synchronization is the first step before conducting demodulation and decoding at a receiver for any wireless communication system. Once an ultrasonic signal packet is detected, it is critically important for the receiver to identify the starting point of the arriving packet. Synchronization can be achieved by correlating the received signal with a known pilot signal being transmitted in front of the information data packets. As widely used in practical radar systems for range detection, a linear frequency modulation (LFM) signal whose frequency increases or decreases linearly with time is used as the pilot for wireless synchronization [13]. The LFM signal in the time domain can be expressed as

$$s(t) = 0.5[1 - \cos(\frac{2\pi t}{T})] \cos[2\pi t(f_0 + \frac{k}{2}t) + \phi], \quad (8)$$

where f_0 is the initial frequency and k is the rate of the frequency change. Note that the LFM signal is multiplied by a Hanning window $0.5[1 - \cos(2\pi t/T)]$ to smooth out the sudden changes in signal amplitude and improve the resolution of the received signal during signal processing. Fig. 3 (a) presents a time-domain LFM signal with a frequency change

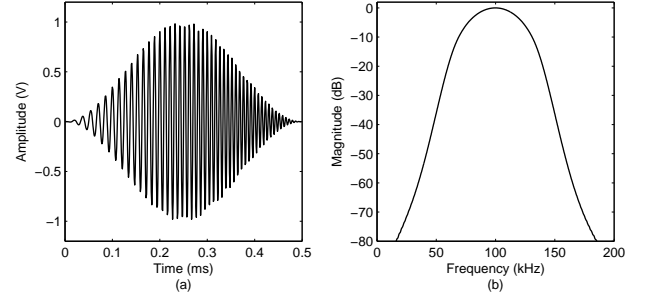


Fig. 3. Hanning windowed LFM signal in (a) time domain; and (b) frequency domain.

from 50 kHz to 150 kHz within 0.5 ms, multiplied by a Hanning window, showing a bell-shaped amplitude with a fade-in and fade-out characteristic. Its frequency spectrum in Fig. 3 (b) shows a concentrated shape without any redundant sidelobes.

By correlating the received signal with a known LFM signal through a matched-filter at the receiver, the highest peak of the matched-filtering output then indicates the first arrival of the transmitted signal. The response of the matched filter to a signal $s(t)$ is defined as

$$g(t) = \int_{-\infty}^{\infty} s(\tau) h(t - \tau) d\tau, \quad (9)$$

whose impulse response is $h(t) = s^*(T - t)$, where $s(t)$ is assumed to be confined to the time interval $[0, T]$. The matched filtering of a received signal $r(t)$ then produces the output signal

$$\begin{aligned} y_{MF}(t) &= \int_{-\infty}^{\infty} r(\tau) h(t - \tau) d\tau \\ &= \int_0^T r(\tau) s^*(\tau) d\tau. \end{aligned} \quad (10)$$

III. APPARATUS AND EXPERIMENTAL LAYOUT

Most ultrasonic transducers used for airborne applications have a bandwidth too narrow to provide an acceptable data rate for wireless communications. There is a capacitive ultrasonic transducer [14] widely available commercially, originally designed by Polaroid as a range finder for autofocus cameras. The ultrasonic transducers used in this work, as shown in Fig. 4, are SensComp series 600 environmental grade with a prominent frequency of 50 kHz. These devices are composed of a gold foil coated polymer membrane and a rigid contoured aluminium backplate with an aperture size of 38.4 mm. The SensComp series 600 capacitive transducers have been used in robotic applications [15], ultrasonic tomography of concrete structures [16], and acoustic separation of suspended submicron solid particles in gases [17].

Additionally, a pair of prototype broadband capacitive ultrasonic transducers were also investigated in the communication system. The custom-made transducer [18], as shown in Fig. 5, had a pitted backplate covered by a metallized PET membrane, and assembled into a screened casing with a 10 mm diameter

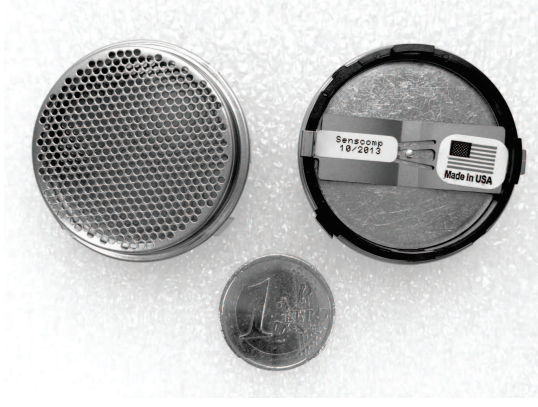


Fig. 4. SensComp series 600 environmental grade ultrasonic transducer.

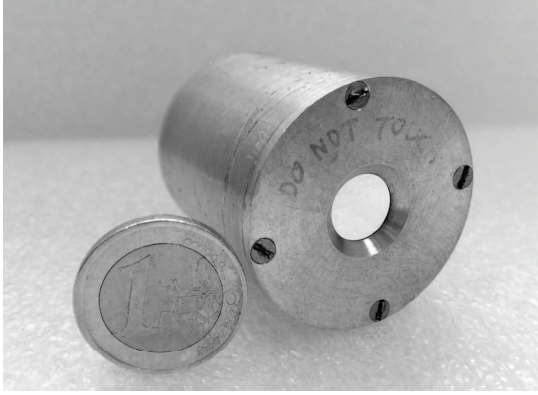


Fig. 5. Laboratory-made air-coupled capacitive ultrasonic transducer.

aperture. Fig. 6 shows a schematic cross-section of the capacitive ultrasonic transducer. The backplate had small symmetric square pyramid shaped air cavity etched into a silicon substrate with edge length $\gamma = 40 \mu\text{m}$, pit separation $\beta = 80 \mu\text{m}$ and sidewall incline $\alpha = 125.264^\circ$. A HfO_2 high- k layer with a thickness of 800 nm was uniformly distributed across the pitted backplate, and covered by a 5- μm metallized polymer film. Here, k is the dielectric constant, and a high- k material allows increased capacitance of a parallel plate capacitor [19].

Fig. 7 illustrates the experimental setup of the ultrasonic communication system. The modulated data signal generated by a PC using MATLAB (The Math Works, Inc.) was uploaded to a TTI TGA 12102 arbitrary waveform generator (Thurlby Thandar Instruments Ltd.) through a GPIB interface before being amplified by a Falco WMA-300 amplifier (Falco Systems B.V.) and superimposed with a bias voltage of +200 V fed by a Delta Elektronika ES 0300-0.45 DC power supply (Delta Elektronika B.V.). The air-coupled ultrasonic signal was detected by a receiver transducer which was connected to a Cooknell CA6/C charge amplifier (Cooknell Electronics Ltd.) with its SU2/C 100 V biasing unit. The voltage signal was then digitized by a PicoScope 6403A PC oscilloscope (Pico Technology), and sent back to the PC through a USB interface for the data analysis.

The system frequency response and phase response when using SensComp transducers over a typical range of 2 m are shown in Fig. 8(a) and (b), respectively. As can be seen in

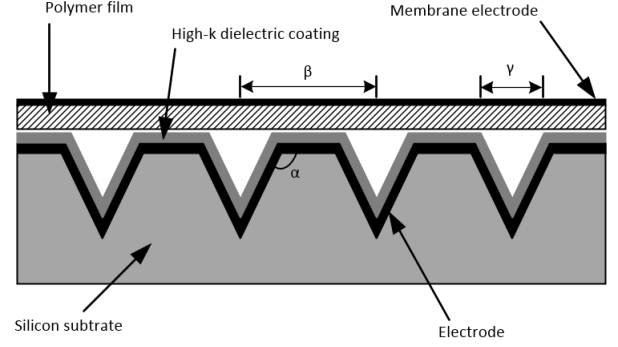


Fig. 6. Schematic cross-section of a high- k capacitive ultrasonic transducer.

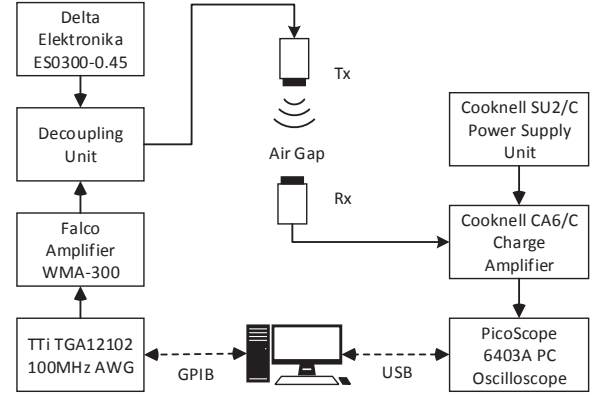


Fig. 7. Experimental setup for a prototype ultrasonic communication system.

Fig. 8(a), the spectrum peaks at about 50 kHz as expected with a dominant response extending to about 115 kHz. It indicates using data channels at ultrasonic frequencies from 46 kHz to 113 kHz is appropriate in terms of 6-dB bandwidth. The phase response of the system in Fig. 8(b) is nearly linear across the 6-dB bandwidth. It means that there is no phase distortion due to the time delay of frequencies relative to one another.

For the high- k transducers, the measured system frequency response over an air channel of 0.5 m is shown in Fig. 9(a). As can be seen, the spectrum peaks at about 260 kHz, with a significant decline in response above 450 kHz. The 6-dB bandwidth is about 220 kHz from 190 kHz to 410 kHz. Fig. 9 (b) shows that the phase response of the channel is nearly linear at frequencies under 650 kHz.

IV. RESULTS AND DISCUSSION

The experiment was carried out in an indoor laboratory with no detectable ultrasonic background noise. The centre normals of the transmitter and receiver transducers were laser aligned to provide a direct line-of-sight (LOS) transmission link. The OFDM symbol T_s was set at 1 ms, giving a subcarrier spacing f_d of 1 kHz in order to retain the orthogonality. Three different baseband modulation methods, BPSK, QPSK and 16-QAM, were used to modulate the subcarrier signals from 55 kHz to 99 kHz using the SensComp transducers, and 200 kHz to 399 kHz using the high- k transducers. Note that Gray coding

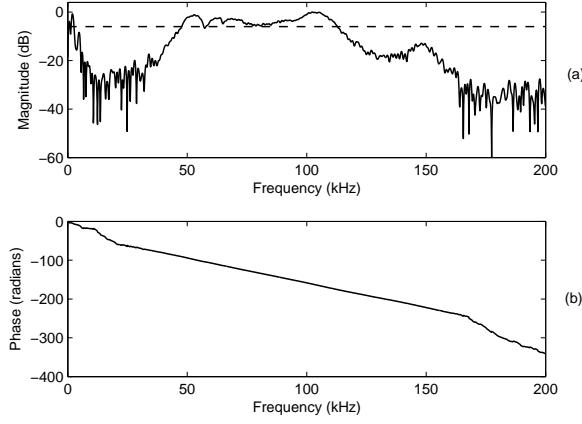


Fig. 8. System characteristics using SensComp transducers over 2 m: (a) frequency response; and (b) phase response.

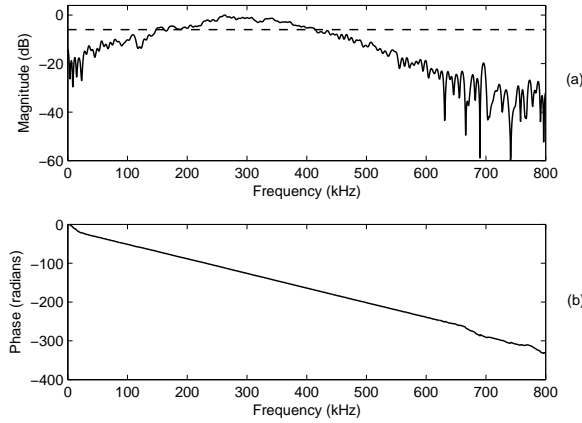


Fig. 9. System characteristics using high- k transducers over 0.5 m: (a) frequency response; and (b) phase response.

was used for generating both QPSK and 16-QAM symbols. This is to minimise the decoding error as every two adjacent symbols differ from each other by only one bit [20]. Due to the memory limitation of the arbitrary waveform generator, only 90 packets of 1-ms OFDM signals were sent through the air channel.

Fig. 10(a) shows a received Hanning-windowed LFM synchronization signal at 10 m with low SNR. The signal had a duration of 1 ms with its frequency swept from 50 kHz to 100 kHz. By performing cross-correlation of a known signal and the received signal in noise using a matched filter, the resulting waveform in Fig. 10(b) shows a large enhancement of SNR which enables a precise and robust detection of the starting point of the incoming signal packets.

Fig. 11 shows the received 16QAM-OFDM signal constellations before and after channel equalisation using SensComp and high- k ultrasonic transducers. Note only 16QAM-OFDM signal constellations are presented as illustrative samples. As can be seen from Fig. 11 (a) and (b), both the constellations are heavily distorted with corrupted phases and amplitudes. After channel equalisation, both constellations in Fig. 11 (c) and (d) form three circular rings with three different openings.

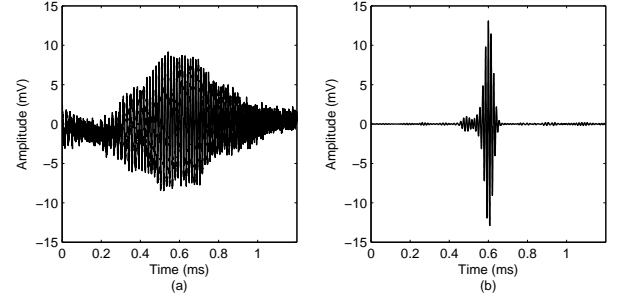


Fig. 10. Wireless synchronization: (a) received LFM signal at 10 m; and (b) its matched filter output.

This is because the amplitudes of the 16 constellation points have three different values $\sqrt{2}$, $\sqrt{10}$ and $3\sqrt{2}$ as shown in Fig. 2 (c). However, the two constellation diagrams indicate that the amplitude distortion has been recovered while the phase distortion is still retained. This phase rotation is introduced by the sampling frequency offset of the Picoscope oscilloscope as the sampling rate of the transmitted OFDM signal was 10 MHz while the actual received signal was sampled at 9.766 MHz. To tackle the sampling frequency offset problem, the received signal was interpolated until it has the same number of samples as that of the transmitted signal as MATLAB can only process integer number of samples. Fig. 12 (a) and (b) show the received constellations when using SensComp and high- k transducers, respectively, after applying interpolation and channel equalisation. As can be seen, the constellations shown in Fig. 12 (a) are well located around their original points when using SensComp devices at relatively low frequency subcarriers. However, in Fig. 12 (b), the constellations of demapped symbols at higher frequencies when using high- k transducers still have a certain amount of group phase rotation which moves part of the constellations across the detection boundaries. It indicates that OFDM signals are more sensitive to phase distortion especially at high frequency channels. This phase rotation is also accumulating with time as the constellations in Fig. 12 (d) show that the last 10 out of 90 OFDM signal packets received have larger phase rotations than the first 10 packets. In comparison, both the first 10 and last 10 packets of the received OFDM signal constellations at low frequencies are clustered within the 16 individual detection regions with negligible phase rotation as shown in Fig. 12 (c). The group phase offsets, $\Delta\phi$, of different OFDM data packets when using both SensComp and high- k transducers were calculated and plotted in Fig. 13. As can be seen, the phase offset of the received signal when using SensComp transducers has a minor increment with time from 0° up to about 1° at the 90th data packet. When using high- k transducers at high frequency subcarriers, the phase offset gradually increases from 0° for the first OFDM packet to approximately 16° when the last packet is received.

To further compensate the phase offset for high-frequency OFDM signals using high- k devices, the pilot signal was periodically inserted between the OFDM data packets. Fig. 14 shows the pilot arrangement used in this work. As can be seen, all subcarriers are used as pilot signals, and the pilots

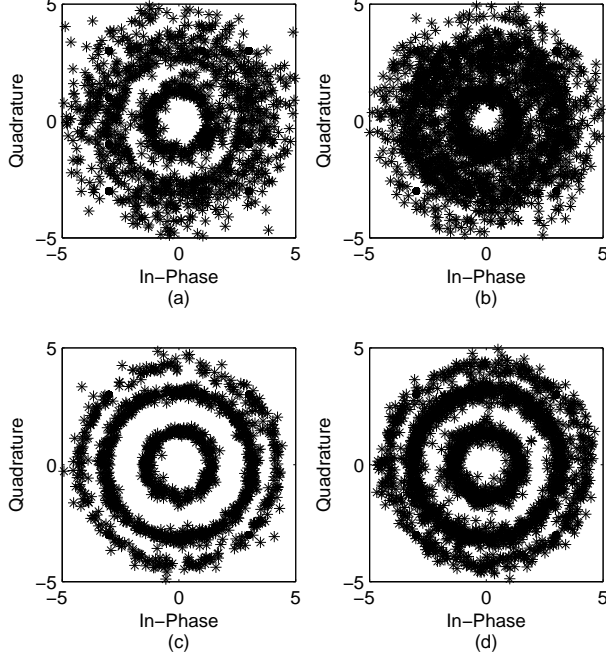


Fig. 11. Received OFDM constellations using SensComp transducers before (a) and after (c) channel equalisation for 16-QAM at 2 m, and constellations using high- k transducers before (b) and after (d) channel equalisation for 16-QAM at 0.5 m.

are inserted every 10 OFDM data packets. This can limit the group phase offset within about 2° which is considered a safe decoding range. However, the overall system data transfer rate is reduced by 10% at the same time after the pilot insertion.

The performances including bandwidth efficiency, data rate, attainable transmission range, SNR and bit error rate (BER) of all three modulation schemes were evaluated and compared using SensComp and high- k ultrasonic transducers in the experiments. The bit errors of the OFDM signals were measured with increasing range, and each 90-packet signal was transmitted 10 times before averaging. The maximum attainable transmission distances with no measurable errors are listed in Table I. As can be seen, higher order modulation schemes have smaller noise margins, therefore requiring much larger SNRs to error-free transmission (i.e. no measurable errors) compared with low-order modulations. The achieved error-free ranges using 16-QAM at low and high frequencies were up to 6 m and 0.7 m, and at 180 kb/s and 800 kb/s, respectively. These ranges were extended to 11 m and 1.2 m when BPSK modulation was used at 45 kb/s and 200 kb/s. Apparently, the most reliable OFDM link was transmitting BPSK modulated signals with the minimum SNR required. But when the system throughput is a priority, 16QAM-OFDM signals which are four times more efficient than that of BPSK-OFDM are suggested for a higher data transfer rate. Besides, as high-frequency ultrasound suffers severe atmospheric absorption in air [21], more energy was needed for a successful signal transmission, and the attainable ranges were also significantly restricted.

To better visualise the received OFDM signal conditions before and after the channel equalization, constellation dia-

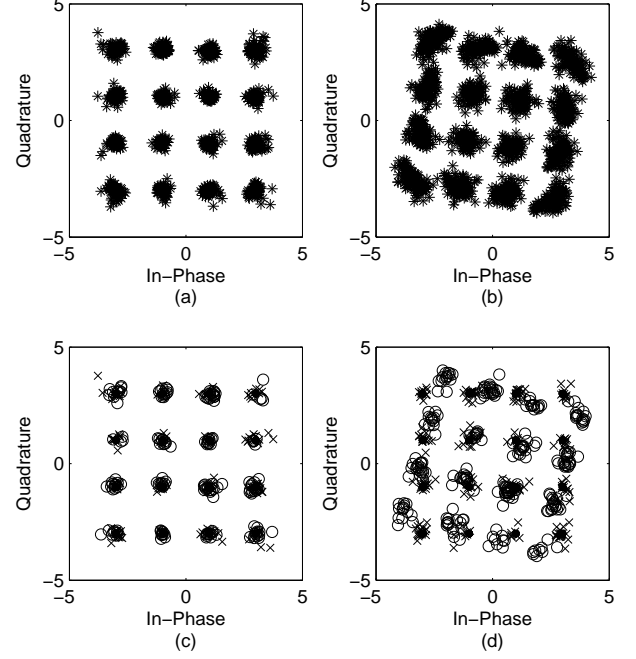


Fig. 12. Received OFDM constellations using (a) SensComp transducers at 2 m and (b) high- k transducers at 0.5 m after interpolation and channel equalisation. (c) and (d) Corresponding signal constellations showing the first 10 (x) and last 10 (o) OFDM data packets.

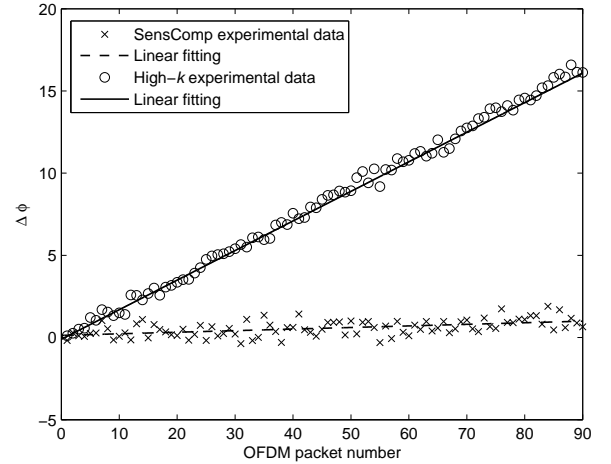


Fig. 13. The trend of the group phase offset when using SensComp and high- k ultrasonic transducers with their individual linear fittings.

grams of BPSK, QPSK and 16-QAM are given in Fig. 15 and Fig. 16 when using the SensComp and high- k transducers, respectively. As can be seen from Fig. 15 (a) - (c), the raw signal constellations after the demodulation process are completely corrupted as a significant amount of demapped symbols have drifted in both phase and amplitude. By analysing the received pilot signal which was previously known by the receiver, the phase and amplitude shifts due to the effect of the ultrasonic channel in air can then be compensated for before decoding. Fig. 15 (d) - (f) illustrate the three constellations after channel equalisation. As can be seen, all constellations

TABLE I
EXPERIMENTAL OFDM TRANSMISSION

Ultrasonic Transducers	Modulation Format	f_c^a (kHz)	Bandwidth (kHz)	Data Rate ^b (kb/s)	Bandwidth Efficiency (b/s/Hz)	Range (m)	SNR (dB)	BER ^c
SensComp	BPSK	77	45	45	1	11	0.63	$<2.47\text{E-}5$
	QPSK			90	2	9	11.78	$<1.23\text{E-}5$
	16-QAM			180	4	6	15.62	$<6.17\text{E-}6$
High- k	BPSK	300	200	200 (180)	1	1.2	12.27	$<5.56\text{E-}6$
	QPSK			400 (360)	2	1.1	15.93	$<2.78\text{E-}6$
	16-QAM			800 (720)	4	0.7	24.69	$<1.39\text{E-}6$

^a Central carrier frequency;

^b Reduced data rate if sampling frequency offset occurs;

^c The values are of BERs with only one bit error.

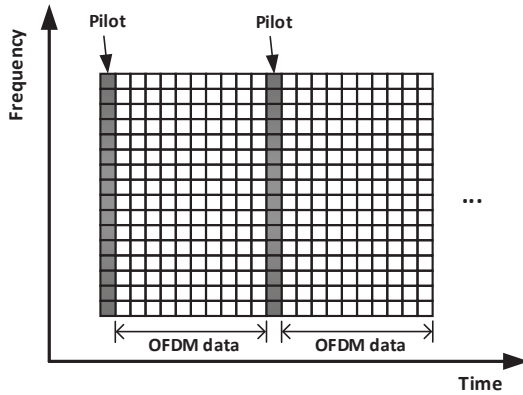


Fig. 14. An illustrative diagram of the pilot arrangement for OFDM signal transmission.

of BPSK, QPSK and 16-QAM are recovered and clustered around their target points. Similarly, when the signals were transmitted and received using high- k ultrasonic transducers, considerable phase and amplitude noise can be observed from the raw received data after the OFDM symbols were demapped as shown in Fig. 16 (a) - (c) for different modulation schemes. Again, Fig. 16 (d) - (f) show three individual well located constellation patterns after channel equalisation as the inserted pilot signal provided the measurement of actual noise at each ultrasonic channel to correct the distortions and separate different constellation points.

V. CONCLUSION

As a highly efficient modulation scheme, OFDM has been investigated in this work for the implementation of an airborne ultrasonic communication system using both commercially available and prototype transducers. The commercially available and prototype ultrasonic transducers have different operating frequency at 77 kHz and 300 kHz, and with bandwidths of 45 kHz and 200 kHz, respectively. Baseband modulations chosen were BPSK, QPSK and 16-QAM, and their performances in terms of data rate, range, spectral efficiency, SNR and BER were evaluated. The results have indicated that a 16-QAM modulation can be used to transmit ultrasonic signals in air at 180 kb/s over a range of 6 m in a LOS manner

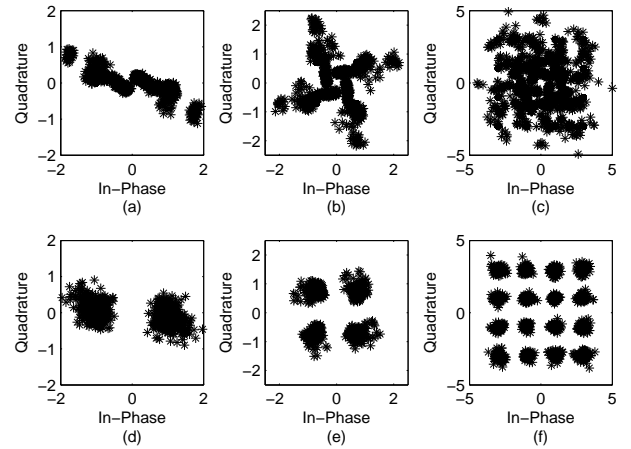


Fig. 15. Received OFDM constellations using SensComp transducers before (a) - (c) and after (d) - (f) channel equalisation for BPSK, QPSK and 16QAM at 11 m, 9 m and 6 m, respectively.

using SensComp transducers, and at 800 kb/s over 0.7 m using high- k transducers. It was also shown that the BPSK approach can provide the most reliable communication link up to 11 m at a reduced system transfer rate of 45 kb/s using SensComp transducers, and 1.2 m at 200 kb/s using high- k transducers. It is also concluded that a trade-off should be made between the attainable range and data transfer rate for airborne ultrasonic communication as the transmission range is significantly restrained by the high-frequency attenuation of ultrasound while at the same time broader bandwidth at high frequency is needed for higher system data rates. Fig. 17 compares this work with the prior airborne ultrasonic data communication systems described in Section I in terms of their data rates and attainable transmission ranges. As can be seen, when SensComp transducers are used for OFDM signal transmission, this work has filled the gaps where the longer ranges and higher data rate are compared with the prior works. By using high- k transducers, this work has also improved the overall system data rate at short ranges. Future studies may include applications for building a practical airborne indoor ultrasonic communication network.

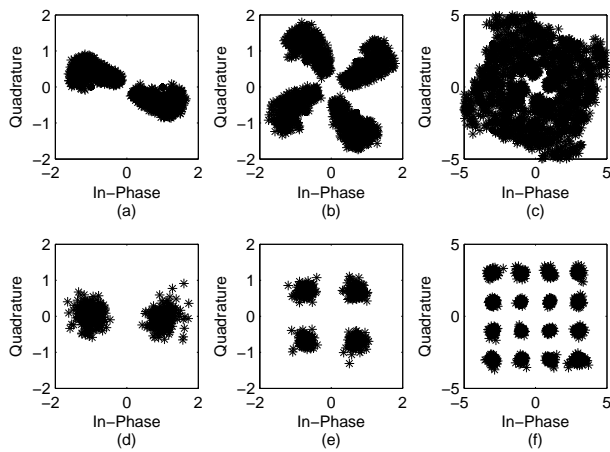


Fig. 16. Received OFDM constellations using high- k transducers before (a) - (c) and after (d) - (f) channel equalisation for BPSK, QPSK and 16QAM at 1.2 m, 1.1 m and 0.7 m, respectively.

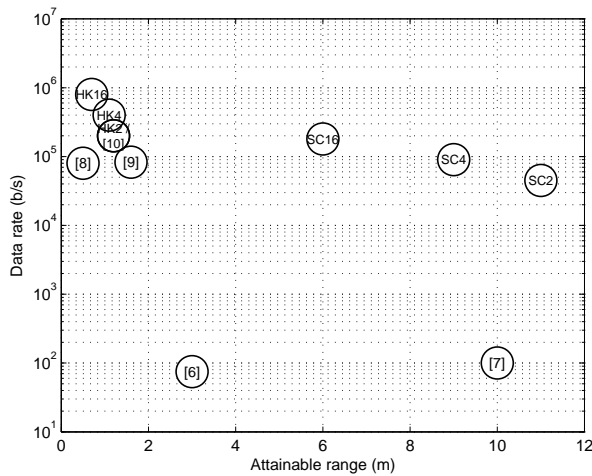
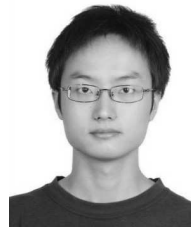


Fig. 17. Comparison of different airborne ultrasonic data communication systems and their data rates at attainable transmission ranges. SC2, SC4 and SC16 represent BPSK-OFDM, QPSK-OFDM and 16QAM-OFDM when using SensComp transducers, respectively, and HK2, HK4 and HK16 represent BPSK-OFDM, QPSK-OFDM and 16QAM-OFDM when using high- k transducers, respectively.

REFERENCES

- [1] I. F. Akyildiz, W.-Y. Lee, M. C. Vuran, and S. Mohanty, "NeXt generation/dynamic spectrum access/cognitive radio wireless networks: A survey," *Comput. Netw.*, vol. 50, no. 13, pp. 2127 – 2159, 2006.
- [2] N. Borisov, I. Goldberg, and D. Wagner, "Intercepting mobile communications: the insecurity of 802.11," in *Proc. 7th Annu. Int. Conf. Mobile Comput. Netw. (MobiCom)*, 2001, pp. 180–189.
- [3] R. Baan, Y. Grosse, B. Lauby-Secretan, F. E. Ghissassi, V. Bouvard, L. Benbrahim-Tallaa, N. Guha, F. Islami, L. Galichet, and K. Straif, "Carcinogenicity of radiofrequency electromagnetic fields," *Lancet Oncol.*, vol. 12, no. 7, pp. 624 – 626, 2011.
- [4] Assemblée Nationale (2016, Aug.), [Online]. Available: <http://www.assemblee-nationale.fr/14/ta/ta0468.asp>.
- [5] S. B. Barnett, G. R. T. Haar, M. C. Ziskin, H.-D. Rott, F. A. Duck, and K. Maeda, "International recommendations and guidelines for the safe use of diagnostic ultrasound in medicine," *Ultrasound Med. Biol.*, vol. 26, no. 3, pp. 355 – 366, 2000.
- [6] H. D. Haynes, M. A. Akeman, and V. M. Baylor, "Ultrasonic communication project, phase 1, FY 1999," Oak Bridge, TN, USA, Tech. Rep., Jun. 2000.

- [7] S. Holm, O. Hovind, S. Rostad, and R. Holm, "Indoors data communications using airborne ultrasound," in *Proc. IEEE Int. Acoust. Speech. Signal (ICASSP)*, vol. 3, 2005, pp. 957–960.
- [8] W. M. D. Wright, O. Doyle, and C. T. Foley, "Multi-channel data transfer using air-coupled capacitive ultrasonic transducers," in *Proc. IEEE Int. Ultrason. Symp. (IUS)*, 2006, pp. 1805–1808.
- [9] C. Li, D. Hutchins, and R. Green, "Short-range ultrasonic digital communications in air," *IEEE Trans. Ultrason., Ferroelectr., Freq. Control*, vol. 55, no. 4, pp. 908–918, 2008.
- [10] —, "Short-range ultrasonic communications in air using quadrature modulation," *IEEE Trans. Ultrason., Ferroelectr., Freq. Control*, vol. 56, no. 10, pp. 2060–2072, 2009.
- [11] W. Jiang and W. M. D. Wright, "Indoor wireless communication using airborne ultrasound and ofdm methods," in *Proc. IEEE Int. Ultrason. Symp. (IUS)*, Sept. 2016, pp. 1–4.
- [12] J. Proakis and M. Salehi, *Digital Communications*. New York, NY, USA: McGraw-Hill, 2008.
- [13] M. Skolnik, *Introduction to Radar Systems*, ser. Electrical engineering series. New York, NY, USA: McGraw Hill, 2001.
- [14] SensComp, Inc. (2016, Aug.). The Senscomp Website, [Online]. Available: <http://www.senscomp.com/pdfs/series-600-environmental-grade-sensor.pdf>.
- [15] A. Jiménez, Álvaro Hernández, J. Ureña, M. C. Pérez, F. J. Álvarez, C. D. Marziani, J. J. García, and J. M. Villadangos, "Emfi-based ultrasonic transducer for robotics applications," *Sensor. Actuat. A: Phys.*, vol. 148, no. 1, pp. 342 – 349, 2008.
- [16] H. Choi and J. S. Popovics, "NDE application of ultrasonic tomography to a full-scale concrete structure," *IEEE Trans. Ultrason., Ferroelectr., Freq. Control*, vol. 62, no. 6, pp. 1076–1085, June 2015.
- [17] R. J. Imani and E. Robert, "Acoustic separation of submicron solid particles in air," *Ultrasonics*, vol. 63, pp. 135 – 140, 2015.
- [18] S. G. McSweeney and W. M. D. Wright, "HfO₂ high- k dielectric layers in air-coupled capacitive ultrasonic transducers," in *Proc. IEEE Int. Ultrason. Symp. (IUS)*, 2011, pp. 864–867.
- [19] G. D. Wilk, R. M. Wallace, and J. M. Anthony, "High- k gate dielectrics: Current status and materials properties considerations," *J. Appl. Phys.*, vol. 89, no. 10, pp. 5243–5275, 2001.
- [20] E. McCune, *Practical digital wireless signals*. Cambridge, U.K.: Cambridge University Press, 2010.
- [21] W. Mason and R. Thurston, Eds., *Physical acoustics: principles and methods*. New York, NY, USA: Academic Press, 1984.



Wentao Jiang (S'14) received the B.Eng. degree in communications engineering from Zhejiang University of Technology, Hangzhou, China, in 2010, and the M.Sc. degree in communications engineering from the University of York, York, U.K., in 2012. He is currently pursuing the Ph.D. degree in air-coupled ultrasonic communication with University College Cork, Cork, Ireland.

His current research interests include capacitive ultrasonic transducers, digital modulation and signal processing.



William M.D. Wright (M'98-SM'10) received the B.Eng. and Ph.D. degrees in mechanical engineering from the University of Warwick, Coventry, U.K., in 1991 and 1996, respectively.

He was a Postdoctoral Researcher with the University of Warwick until 1997, when he joined the School of Engineering, University College Cork, Cork, Ireland, where he is currently a Senior Lecturer in Mechanical Engineering. His current research interests include noncontact ultrasonic measurements, design and development of capacitive ultrasonic transducers, ultrasonic flow metering in gases, and ultrasonic communications.

Dr. Wright is a member of the Acoustical Society of America and an Associate Editor of the IEEE Transactions on Ultrasonic, Ferroelectrics, and Frequency Control.